Turkish Journal of Electrical Engineering & Computer Sciences

http://journals.tubitak.gov.tr/elektrik/

Research Article

Turk J Elec Eng & Comp Sci
(2014) 22: 243 – 261

doi:10.3906/elk-1203-49

Concurrently attuned design of a WADC-based UPFC PSDC and multiinput PSS for improving power system dynamic performance

Yashar HASHEMI, Rasool KAZEMZADEH*, Mohammad Reza AZIZIAN, Ahmad SADEGHI YAZDANKHAH
Electrical Engineering Faculty, Sahand University of Technology, Tabriz, Iran

Received: 13.03.2012 • **Accepted:** 27.08.2012 • **Published Online:** 17.01.2014 • **Printed:** 14.02.2014

Abstract: A new controller design for a unified power flow controller (UPFC) for damping of power system swings, focusing on interarea modes, is described in this paper. The proposed controller is a dual-layer controller, where the first layer is derived from local signals and the second layer is supplied by global signals, as additional measuring information from suitable remote network locations, where swings are well observable. For damping of low-frequency swing in wide-area operation, since there is little system information in the active power as input of the conventional power system stabilizer (CPSS), the effectiveness of the CPSS is low. For solving this problem, a multiinput power system stabilizer (MPSS) is used for the damping of low-frequency swings, where the choice of the MPSS location is based on modal analysis. Since an uncoordinated controller for the UPFC and MPSS may cause unwanted interactions, the concurrently attuned design of the controller parameters is necessary. The attuned design is presented as an optimization problem, where the particle swarm optimization algorithm is applied to search for the optimal controller parameters. The introduced time delay by remote signal transmission and processing in a wide-area damping controller (WADC) may be problematic for system stability and may decrease system robustness. The Lyapunov theory and model reduction technique are used to investigate the delay-dependent stability of a power system equipped with a WADC. The designed controller's effectiveness and robustness are investigated on a typical 2-area 4-machine benchmark power system.

Key words: UPFC, power swing damping controller, wide-area damping controller, dual-layer UPFC damping controller, concurrently attuned

1. Introduction

Steadily increasing incidents of fault/disturbances can affect modern power networks and cause to interarea rotor angle and power swings. Compared to the local swing modes that are effectively determined and influenced by the local-area states, the interarea modes are more complicated to study, since they need a detailed model of the system as a whole and are affected by the global states of large areas in the power systems. A locally tuned and designed power system stabilizer (PSS) usually fails to act effectively during the interarea swings. An exactly tuned PSS may also be useful in damping the interarea modes up to a limited transmission loading. Interarea mode damping is limited because these modes are not effectively controllable and observable in the generator's local signals. Moreover, in the system, the number of dominant modes is much larger than the number of available controlled devices. Hence, the traditional method of having a PSS tuned for a local mode and also a certain interarea mode might not be sufficient for ensuring the stability of the system.

*Correspondence: r.kazemzadeh@sut.ac.ir

Among the generator exciter control methods for stability enhancement, PSS-based active power, as the input signal, is widely used. The method suppresses the local power swings between generators. With regard to the minor information contained in the active power signal, low-frequency swing damping is nonsignificant in this method. To solve the disadvantage of the conventional PSS, rotor speed deviation, as the input signal, is also used along with the active power input [1–3].

In addition to the PSS, flexible AC transmission system (FACTS) devices are implied to enhance system stability [4–8]. Specifically, in multimachine power systems, using only a PSS may not provide effective damping for interarea swings. In these cases, FACTS power swing damping controllers (PSDCs) are effective solutions. Power swing damping with FACTS devices is affected by power modulations using a supplementary damping controller. The device is named a FACTS device stabilizer. On the other hand, the uncoordinated local control of PSSs and FACTS devices always causes destabilizing interactions. To enhance the overall system performance, many researchers have concentrated on the coordination between PSSs and FACTS PSDCs [9–12]. Some of these coordination methods are based on a complex nonlinear simulation [9,13], and the others use a linearized power system model.

Although FACTS, PSDCs, and multiinput PSSs (MPSSs) play an effective role in damping the interarea swings because these controllers normally use local inputs, they cannot always be effective in easing the damping problem. Local controllers lack the global observation of the interarea modes. It has been demonstrated that under some operating conditions, an interarea mode may be controllable in one area and observable in another [14]. In such cases, local controllers are not effective for the damping of this mode.

Several references presented that, due to the lack of observability in local measurements of some interarea modes, damping control using global signals may be more effective than local control [15–17]. The wide-area control technologies suggest a great ability to overcome the shortcomings of conventional local controllers. Using a global positioning system-based phasor measurement unit, the dynamic parameters of power systems (such as voltage, current, angle, and frequency) can be accurately measured, synchronized, and transferred over the whole power network by wide-area measurement systems [18,19]. This provides the possibility of constructing wide-area damping control systems. An application of a wide-area control system (WACS) using global measurements is a wide-area damping controller (WADC). This approach corresponds to a controller design that uses wide-area measurements to enhance power system swing damping. The WADC implementation, such as the control of PSSs using synchronized phasor measurements in [20,21], has been discussed. One of the main disadvantages of WACSs in communication links is a large time delay. The delay between the measurement instant and the instant signal being available to the controller is normally in the range of 0.1 s to 0.7 s [22], which depends on the distance, transmission protocol, and several other factors. As the delay is comparable to the time periods of some critical interarea swing modes, it should be considered in the design stage.

This paper extends the use of global control signals in the designing of a unified power flow controller (UPFC) PSDC in coordination with a MPSS. The proposed UPFC controller for power swing damping is a dual-layer UPFC damping controller, in which its first layer is derived from local signals and the second one is supplied from global signals. The dual-layer UPFC damping controller with MPSS controllers is tuned to simultaneously move the undamped electromechanical modes to a predetermined zone. The attuned design of the MPSS and the proposed UPFC controller is presented as an optimization problem, according to the eigenvalue-based objective function comprising the real part of the eigenvalue and the damping ratio of the undamped electromechanical modes. This problem is solved using the particle swarm optimization (PSO) technique that has the ability to search the most optimistic results. The second layer of the UPFC controller is called a UPFC-WADC,

which uses both wired (telephone lines, fiberoptics) and wireless (satellites) communication links. In this paper, remote signal transmission time delay, based on the Lyapunov theory and model reduction technique, has been considered for UPFC-WADC designing. The effectiveness and ability of the proposed controllers is tested on a typical 2-area 4-machine benchmark power system using MATLAB software, and a comparative study between the results of the dual-layer UPFC and MPSS, and the conventional UPFC (CUPFC) and MPSS design is presented.

2. Test system description

The modified 2-area 4-machine system is used to validate the proposed dual-layer UPFC damping controller. From Figure 1 it is seen that the UPFC controller is applied to improve the interconnected ability of the 2 areas. The results of many research works show that there is a typical interarea swing mode between the 2 areas. For this swing damping, the rotor speeds of the generators are chosen as the wide-area feedback control inputs for the UPFC-WADC. The 2-area 4-machine network was created to present the different types of swings that occur in both large and small interconnected power systems. Detailed model descriptions were given in ..[23] and Appendix A. All of the synchronous machines are considered with a static excitation system and MPSS with 2 lead-lag compensation blocks for every input. The exported power P_{tie} from area 1 to area 2 through the tie line is 460 MW and is chosen as the nominal operating condition. It is varied in the range of 0 to 500 MW, by varying the loads and generation in each area.

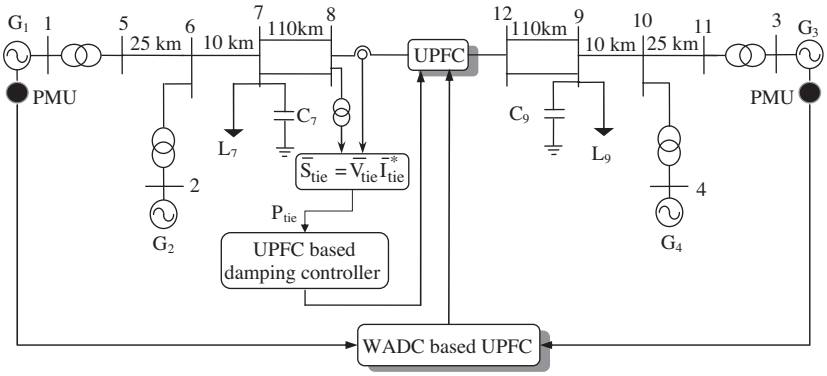

Figure 1. Modified 2-area 4-machine test system equipped with a UPFC.

3. Model of the multimachine power system equipped with a UPFC

A multimachine power system equipped with a UPFC is described for this study. In some papers, the dynamic model of the multimachine power system with a UPFC was developed [5,24]. In this paper, the proposed method in [5] is used. Figure 2 shows a multimachine power system with a UPFC. The UPFC performance is based on the pulse width modulation technique of the converter. In this figure, m_E, m_B and δ_E, δ_B are the amplitude modulation ratios and phase angles of the reference voltage in each voltage source converter, respectively, and they are the input control signals of the UPFC. For consideration of the effect of the UPFC in the damping of the low-frequency swing, the dynamic model of the UPFC is applied, in which the resistance and transient of the transformers of the UPFC can be ignored. It is considered that a UPFC is installed at buses 1 and 2 in the power system, as shown in Figure 2. For developing the dynamic model of the system, the network is represented by taking out the buses connecting the lines in which the UPFC is installed.

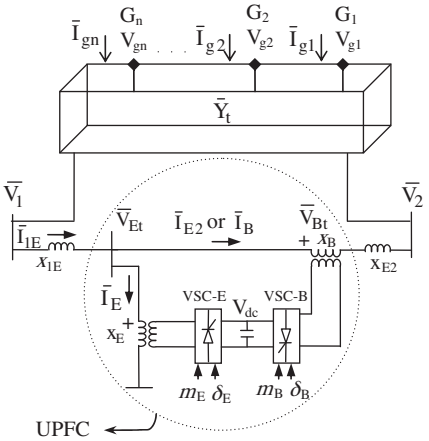

Figure 2. An n-machine power system equipped with a UPFC.

The network admittance $\bar{Y}_t$ is formed before installing the UPFC, keeping n generator nodes along with nodes 1 and 2. The equation of the network is:

$$\begin{bmatrix} 0 \\ 0 \\ \bar{I}_g \end{bmatrix} = \begin{bmatrix} \bar{Y}_{11} & \bar{Y}_{12} & \bar{Y}_{13} \\ \bar{Y}_{21} & \bar{Y}_{22} & \bar{Y}_{23} \\ \bar{Y}_{31} & \bar{Y}_{32} & \bar{Y}_{33} \end{bmatrix} \begin{bmatrix} \bar{V}_1 \\ \bar{V}_2 \\ \bar{V}_g \end{bmatrix} = \bar{Y}_t \begin{bmatrix} \bar{V}_1 \\ \bar{V}_2 \\ \bar{V}_g \end{bmatrix}, \tag{1}$$

where

$$\bar{I}_g = \begin{bmatrix} \bar{I}_{g1} & \bar{I}_{g2} & \dots & \bar{I}_{gn} \end{bmatrix}^T$$
$$\bar{V}_g = \begin{bmatrix} \bar{V}_{g1} & \bar{V}_{g2} & \dots & \bar{V}_{gn} \end{bmatrix}^T .$$

With the installation of a UPFC between buses 1 and 2, the network equation is modified as follows:

$$\begin{cases} \bar{Y'}_{11}\bar{V}_1 + \bar{I}_{1E} + \bar{Y}_{13}\bar{V}_g = 0 \\ \bar{Y'}_{22}\bar{V}_1 - \bar{I}_{E2} + \bar{Y}_{23}\bar{V}_g = 0 \\ \bar{Y}_{11}\bar{V}_1 + \bar{Y}_{32}\bar{V}_2 + \bar{Y}_{33}\bar{V}_g = \bar{I}_g \end{cases}, \tag{2}$$

where $\bar{Y}'_{11}$ and $\bar{Y}'_{22}$ are obtained from $\bar{Y}_{11}$ and $\bar{Y}_{22}$ by excluding $x_{12} = x_{1E} + x_{E2}$.

From Figure 2, we have:

$$\begin{cases} \bar{V}_1 = jx_{1E}I_{1E} + \bar{V}_{Et} \\ \bar{V}_{Et} = jx_{E2}I_{E2} + \bar{V}_{Bt} + \bar{V}_2 \\ \bar{I}_E = \bar{I}_{1E} - \bar{I}_{E2} \end{cases} \tag{3}$$

and for the UPFC:

$$\begin{cases} \bar{V}_E = \frac{m_E V_{DC}}{2} e^{j\delta_E}, \ \bar{V}_B = \frac{m_B V_{DC}}{2} e^{j\delta_B} \\ \bar{V}_{Et} = jx_E\bar{I}_E + \bar{V}_E, \ \bar{V}_{Bt} = jx_B\bar{I}_B + \bar{V}_B \end{cases} \tag{4}$$

$$\frac{dV_{dc}}{dt} = \frac{3m_E}{4C_{dc}} \begin{bmatrix} \cos\delta_E & \sin\delta_E \end{bmatrix} \begin{bmatrix} i_{Ed} \\ i_{Eq} \end{bmatrix} + \frac{3m_B}{4C_{dc}} \begin{bmatrix} \cos\delta_B & \sin\delta_B \end{bmatrix} \begin{bmatrix} i_{Bd} \\ i_{Bq} \end{bmatrix}. \tag{5}$$

Substituting Eq. (4) into Eq. (3) and solving for currents, we have:

$$\begin{cases} \bar{I}_E = \frac{1}{x_\Sigma}\left[-j\left(x_{E2}+x_B\right)\bar{V}_1 - jx_{1E}\bar{V}_2 + \left(x_{1E}+x_{E2}+x_B\right)\bar{V}_E - jx_{1E}\bar{V}_B\right] \\ \bar{I}_{E2} = \frac{1}{x_\Sigma}\left[-jx_E\bar{V}_1 + j\left(x_{1E}+x_E\right)\bar{V}_2 - jx_{1E}\bar{V}_E + j\left(x_{1E}+x_E\right)\bar{V}_B\right] \end{cases}, \tag{6}$$

where $x_\Sigma = \left(x_{1E}+x_E\right)\left(x_E+x_{E2}+x_B\right) - x_E^2$.

Substituting Eq. (6) into Eq. (2) and deleting nodes 1 and 2, results in:

$$\bar{I}_g = \bar{C}\bar{V}_g + \bar{F}_E\bar{V}_E + \bar{F}_B\bar{V}_B. \tag{7}$$

3.1. Nonlinear model of the multimachine power system equipped with a UPFC

The nonlinear model of the multimachine power system with a UPFC is developed as follows:

$$\begin{cases} \dot{\delta} = \omega_0\omega \\ \dot{\omega} = M^{-1}(T_M - T_E - D\omega) \\ \dot{E'}_q = T_{DO}^{'-1}\left[\left(X_D - X'_D\right)I_D - E'_q + E_{fd}\right] \\ \dot{E}_{fd} = \left(T_A^{-1} - E_{fd} + K_A\left(V_{ref} - V_T\right)\right) \end{cases}, \tag{8}$$

where

$$\begin{cases} T_E = I_Q V_{TQ} + I_D V_{TD} \\ V_{TD} = X_Q I_Q, V_{TQ} = \dot{E}'_q - X_D I_D \end{cases} \tag{9}$$

$$\delta = \begin{bmatrix} \delta_1 & \delta_2 & \dots & \delta_n \end{bmatrix}^T$$

$$\omega = \begin{bmatrix} \omega_1 & \omega_2 & \dots & \omega_n \end{bmatrix}^T$$

$$E'_q = \begin{bmatrix} E'_{q1} & E'_{q2} & \dots & E'_{qn} \end{bmatrix}^T$$

$$E_{fd} = \begin{bmatrix} E_{fd1} & E_{fd2} & \dots & E_{fdn} \end{bmatrix}^T$$

$$I_D = \begin{bmatrix} I_{d1} & I_{d2} & \dots & I_{dn} \end{bmatrix}^T$$

$$I_Q = \begin{bmatrix} I_{q1} & I_{q2} & \dots & I_{qn} \end{bmatrix}^T$$

$$V_{TD} = \begin{bmatrix} V_{d1} & V_{d2} & \dots & V_{dn} \end{bmatrix}$$

$$V_{TQ} = \begin{bmatrix} V_{q1} & V_{q2} & \dots & V_{qn} \end{bmatrix}^T$$

$$M = Diag(2H_i), \quad D = Diag(2D_i), \quad T'_{DO} = Diag(T'_{doi}),$$

$$X_D = Diag(x_{di}), \quad X'_D = Diag(x'_{di}), \quad T_A = Diag(T_{Ai}), \quad K_A = Diag(K_{Ai}),$$

and $i = 1, 2, \ldots, n$, where n is the number of generators. For the n machine power system, the terminal voltage of the generators can be expressed in the common coordinates as:

$$\bar{V}_g = \bar{E}'_q - jX'_D\bar{I}_g - j(X_Q - X'_D)\bar{I}_Q. \tag{10}$$

Substituting Eq. (10) into Eq. (7) gives:

$$I_g = \bar{C}_d\left[\bar{E}'_q - j\left(X_Q - X'_D\right)\bar{I}_Q + \bar{C}_E\bar{V}_E + \bar{C}_B\bar{V}_B\right], \tag{11}$$

where

$$\begin{cases} \bar{C}_d = \left(\bar{C}^{-1} + jX'_D\right)^{-1} = C_{dik}e^{j\beta_{dik}} \\ \bar{C}_E = \bar{C}^{-1}\bar{F}_E = C_{Ek}e^{j\beta_{Ek}} \\ \bar{C}_B = \bar{C}^{-1}\bar{F}_B = C_{Bk}e^{j\beta_{Bk}} \end{cases}.$$

In $d-q$ axis form, the generator currents in Eq. (11) can be expressed as:

$$\bar{I}_{Gi} = \bar{I}_{gi}e^{j\delta_i} = \sum_{k=1}^{n}\bar{C}_{dik}\left[E'_{qk}e^{j(90+\delta_k-\delta_i)} + \left(x_{qk} - x'_{dk}\right)e^{j(\delta_k-\delta_i)}I_{qk} + \bar{C}_{Ek}\bar{V}_E e^{j\delta_i} + \bar{C}_{Bk}\bar{V}_B e^{j\delta_i}\right]. \tag{12}$$

3.2. State space form of the linearized model of a multimachine power system equipped with a UPFC

The linear dynamic model of the multimachine power system including the UPFC is achieved by linearizing the nonlinear equations around an operating point of the power system. The modified Heffron-Philips model of the multimachine power system equipped with a UPFC in the state equation form is:

$$\dot{x} = Ax + Bu \tag{13}$$

$$x = \left[\begin{array}{ccccc} \Delta\delta & \Delta\omega & \Delta E'_q & \Delta E_{fd} & \Delta V_{dc} \end{array}\right]^T$$
$$u = \left[\begin{array}{ccccc} \Delta u_{pss} & \Delta m_E & \Delta\delta_E & \Delta m_B & \Delta\delta_B \end{array}\right]^T,$$

where A is the state matrix and B the input matrix [5].

4. Proposed dual-layer UPFC damping controller

The newly designed UPFC controller aims to improve the damping of poorly damped interarea modes. This provides a control signal, which is the sum of 2 control signals. Interarea modes normally have high observability in view of the tie-line's active power between the areas contained in these interarea swings. Hence, the tie-line's active power can be applied as a stabilizing signal for damping the interarea modes associated with this tie-line.

Interarea modes are more complicated to study, as they need the detailed model of the entire interconnected system and are affected by the global states of a larger area in the power network; hence, the global signal can influence the damping of interarea modes. As a WADC-based UPFC uses a global signal as a controller input signal, it can be used to enhance the damping of interarea modes [25]. The residue R_{ij}, related to the speed deviation signal of generator j to control mode i, may not be large enough to achieve satisfactory damping. To increase the residue magnitude based on Eq. (14), either the observability or the controllability

of these modes at the machines must be increased [26,27]. Controllability can be improved by increasing the exciter forward gain. However, this is not always a good scheme, since it can reduce the stability margin for the local mode.

$$|R_{ij}| = |C_j t_i v_i B_j| = obsv_{ij} * cont_{ij}, \tag{14}$$

where the controllability of mode i from the jth input is:

$$cont_{ij} = v_i B_j, \tag{15}$$

and the observability of mode i from the jth input is:

$$obsv_{ij} = C_j t_i. \tag{16}$$

The columns of matrix t as t_i are the right eigenvectors related to the ith mode, and similarly, the rows of matrix v as v_i are the left eigenvectors related to the ith mode.

As the right eigenvector elements correspond to the speed, the observability vectors of 2 machines, j and k, in the generator group oscillating against each other (in an interarea mode) are always about 180° apart. This indicates that the observability of the interarea mode corresponding to the speed difference signal of these 2 machines will be larger in magnitude than any other individual observability. If interarea mode i is controlled by the speed difference signal of machines j and k, then:

$$\Delta\omega_{jk} = \Delta\omega_j - \Delta\omega_k. \tag{17}$$

The observability index for this signal is given by:

$$obsv\left(\Delta\omega_{jk}\right) = C_j t_i - C_k t_i = \left(C_j - C_k\right) t_i,$$

and the total control signal as shown in Figure 3 becomes:

$$V_s = H_{UPFC1}\Delta P_{tie} + H_{UPFC2}\Delta\omega_{jk}. \tag{18}$$

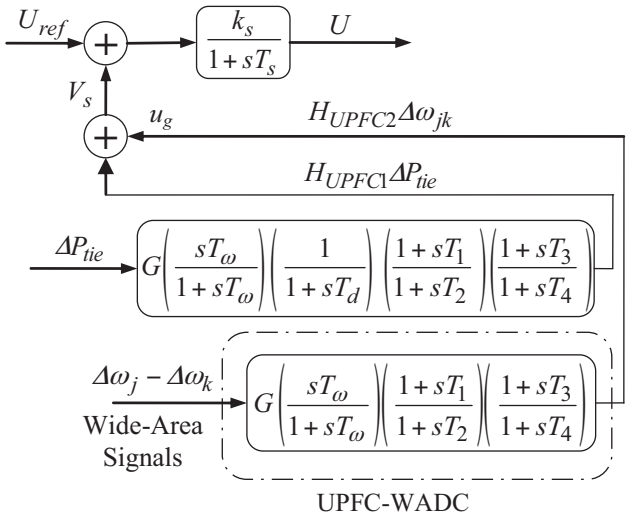

Figure 3. Proposed dual-layer UPFC- PSDC structure.

The eigenvalue and observability analysis of the open-loop system in Table 1 shows one interarea mode. Table 1 gives the frequency, damping ratio, and observability for this interarea mode. From this table it is shown that the observability of the interarea mode using the difference in the signals of machines 1 and 3 is larger in magnitude than the other machines' speed difference signals. Hence, $\omega_1 - \omega_3$ is used as the wide-area signal for the UPFC-WADC.

Table 1. The interarea mode observability using the speed deviation signal.

Interarea mode		Observability of the speed difference signal			
0.1744 ± 4.9583i		ω_1 - ω_3	ω_1 - ω_4	ω_2 - ω_3	ω_2 - ω_4
Freq.	Damping ratio	**0.29**	0.13	0.09	0.17
0.78	–0.0352				

5. Time-delay of wide-area signals

In the design of a WADC, an unavoidable problem is the delay involved between the measurement instant and the time that the signal becomes available to the controller. The time delay decreases the efficiency of the damping control system, and in some cases, large delays destabilize the system, and this should be considered in the controller design procedure so that the designed controller can handle a range of time-delays [25]. These time-delays are caused by measurement processing, synchronization, and control signal calculation and transmission. To restore the performance of the controller in these researches, 2 methods of solutions have been adopted. The first method is a robust controller design based on the Lyapunov stability criterion to keep the system stable under delayed conditions. From this point of view, the linear matrix inequality (LMI) theory is used in stability analysis and the robust controller design of time-delay systems [28,29]. In [29], the Padé approximation by a rational polynomial was used to replace the delay item, and an LMI-based robust controller has been introduced based on the new state matrix without a delay item. In [29], the authors presented a gain scheduling approach based on the LMI to reduce the perverse effect of the time delays. The other method of solution is to perform a prediction or compensation method for delay elimination effects.

In this paper, for time-delay effect consideration on the stability of a system equipped with a WADC, the method in [30] is used. Therefore, to find the maximal delay time defined as a delay margin, its main idea is reviewed briefly in this section.

For a linearized power system excluding the WADC:

$$\begin{cases} \dot{x}(t) = Ax(t) + Bu(t) \\ y(t) = Cx(t) \end{cases}. \tag{19}$$

For a large-scale power system, the order of the linearized model is comparatively high, which makes the design of a controller difficult or even impracticable. Hence, a model reduction method is always used to reduce the order of the entire power system. The 'Schur' model-reduction procedure [31] is used to find the reduced-order system. The reduced-order model of the power system can be presented as follows:

$$\begin{cases} \dot{x}_1(t) = A_1x_1(t) + B_1u(t) \\ y(t) = C_1x_1(t) \end{cases}. \tag{20}$$

The state space form of any linear damping controller can be represented as:

$$\begin{cases} \dot{x}_2(t) = A_2 x_2(t) + B_2 u(t) \\ y_2(t) = C_2 x_2(t) + D_2 u_2(t) \end{cases}. \tag{21}$$

The connections between the reduced-order power system and the WADC are given by:

$$\begin{cases} u_2(t) = y(t - d(t)) \\ u(t) = y_2(t) \end{cases}, \tag{22}$$

where $d(t)$ is the time varying delay and the constant time-delay is denoted as d. In a delay-dependent system, asymptotic stability is kept for $d\langle\tau_d$ and the system is unstable for $d\rangle\tau_d$. Parameter τ_d is a special time delay named a delay margin, which is a critical parameter in evaluating the stability of the delay-dependent system.

The closed-loop power system model with an integrated time-delay can be presented as:

$$\dot{x}(t) = Ax(t) + A_d x(t - d(t)), \tag{23}$$

where $x = [x_1, x_2]^T$, $A = \begin{bmatrix} A_1 & B_1C_2 \\ 0 & A_2 \end{bmatrix}$, and $A_d = \begin{bmatrix} B_1D_2C_1 & 0 \\ B_2C_1 & 0 \end{bmatrix}$.

By considering a system with a time-varying delay as follows:

$$\begin{cases} \dot{x}(t) = Ax(t) + A_d x(t - d(t)),\ t\rangle 0 \\ x(t) = \varphi(t),\ t \in [-\tau, 0] \end{cases}, \tag{24}$$

where $x(t) \in R^n$ is the state vector and $\varphi(t)$ is a vector that consists of continuous valued functions in the range of $t \in [-\tau, 0]$. Parameter $d(t)$ is the time delay that is a continuous function of time and satisfies:

$$0 \le d(t) \le \tau,\ \left|\dot{d}(t)\right| \le \mu \le 1, \tag{25}$$

where τ and μ are the upper bound of the time delay and its rate, respectively. For a constant time delay, $\mu = 0$ and $d(t) = d = \tau$, and for a time-varying delay, $\mu \neq 0$.

Theorem System Eq. (24) is asymptotically stable if there exists symmetric positive-definite matrices $P = P^T\rangle 0$, $Q = Q^T\rangle 0$, and $Z = Z^T\rangle 0$, a symmetric semidefinite matrix $X = \begin{bmatrix} X_{11} & X_{12} \\ X_{12}^T & X_{22} \end{bmatrix} \ge 0$, and any appropriately dimensioned matrices Y and T, such that the following LMI is satisfied [30]:

$$\Phi = \begin{bmatrix} \Phi_{11} & \Phi_{12} & \tau A^T Z \\ \Phi_{12}^T & \Phi_{22} & \tau A_d^T Z \\ \tau ZA & \tau ZA_d & -\tau Z \end{bmatrix} \langle 0, \tag{26}$$

$$\Psi = \begin{bmatrix} X_{11} & X_{12} & Y \\ X_{12}^T & X_{22} & T \\ Y^T & T^T & Z \end{bmatrix} \ge 0, \tag{27}$$

where

$$\begin{cases} \Phi_{11} = PA + A^T P + Y + Y^T + Q + \tau X_{11} \\ \Phi_{12} = PA_d - Y + T^T + \tau X_{12} \\ \Phi_{22} = -T - T^T - (1-\mu)Q + \tau X_{22} \end{cases}.$$

The theorem provides adequate stability of system Eq. (24) for a given μ, and cannot be used directly to attain the delay margin. For a given μ, by manually increasing the value of τ and verifying the feasibility, the delay margin τ_d, which is equal to the maximum τ, can be found. For the existence of the delay margin verification based on the LMI constrains given in the theorem, the function 'feasp' in the MATLAB\LMI control toolbox is used.

6. MPSS

Suitably tuned PSSs can enhance power system stability by damping of the swing modes. They will produce a control signal in phase with the generator rotor speed deviation that causes damping of the low-frequency swing in participating generators. The input of the PSS can be one of the local signals as the generator's speed deviation, accelerating power, or any other appropriate signal [32]. These stabilizers, with a lead-lag compensator or any other compensator, create a portion of electrical torque in phase with the generator's rotor speed deviation. As mentioned before, the rotor speed deviation as the input signal of the PSS, along with the active power signal, is used to not only damp the low-frequency power system swings, but also suppress the local swings [1,2]. These 2 signals are gathered after crossing the compensators and the resultant signal is applied to the PSS, which can vastly improve stability. Therewith, the voltage and reactive power are employed instead of the speed signal. Since the frequency signal or speed signal can be detected from the voltage and current by computation, it does not require any electromagnetic sensors.

The $p+\omega$ input PSS is shown in Figure 4, where p and ω are the generator's local signals, which are selected as the PSS input (Δu_{PSS} in Figure 4). If the p and ω inputs of the PSS are optimized independently and combined to form the $p+\omega$ input of the PSS, an unexpected unstable swing mode may occur. In this paper, the input parameters p and ω of the MPSS with the parameters of the UPFC controller are optimized all together.

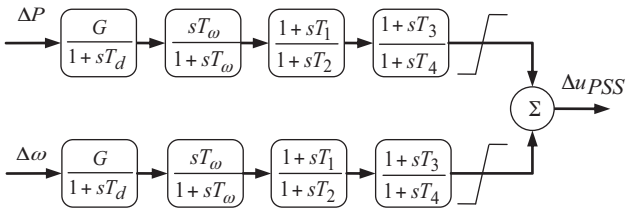

Figure 4. MPSS.

7. Modal analysis and MPSS placement

The MPSS placement plays an important role in the ability of a device to stabilize a swing mode [33,34]. Many researches or indices based on an open-loop system model have been presented and successfully used to guide damping controller placement. The residue method achieved from the modal control theory of linear time-invariant systems (which can direct the controllability and/or observability of a device) can cause effective location selection. According to Eq. (14), residues give the sensitivity of the corresponding eigenvalue to

feedback the transfer function output to its input. They are useful in finding the feedback signal, which gives the largest influence on the research mode. From the open-loop system eigenvalue and residue analysis shown in Tables 2 and 3, the system exhibits 2 local modes and 1 interarea mode. The frequency, damping ratio, and residues for these modes are shown in Tables 2 and 3, where it can be seen that the local and interarea modes are more sensitive to generators 1 and 3, and can be improved by installing a MPSS.

Table 2. The residues related to the local and interarea modes (speed signal).

Electromechanical modes	Freq.	Damping ratio	Machines participation factor			
			$\Delta\omega_1$	$\Delta\omega_2$	$\Delta\omega_3$	$\Delta\omega_4$
–0.6450 ± i6.3493	1.011	0.0995	**0.0271**	0.0012	0.011	0.0019
–0.2682 ± i5.0935	0.811	0.0526	0.0115	0.0001	**0.0314**	0.0166
0.1744 ± i4.9583	0.78	–0.0352	**0.0300**	0.0052	0.0164	0.001

Table 3. The residues related to the local and interarea modes (power signal).

Electromechanical modes	Freq.	Damping ratio	Residue			
			ΔP_1	ΔP_2	ΔP_3	ΔP_4
–0.6450 ± i6.3493	1.011	0.0995	**8.0970**	0.4680	0.0096	0.8604
–0.2682 ± i5.0935	0.811	0.0526	3.4477	0.0055	**11.9447**	7.6428
0.1744 ± i4.9583	0.78	–0.0352	**13.7963**	1.5668	6.2458	0.0097

8. The best UPFC input signal selection using the controllability measurement

To measure the controllability of each electromechanical (EM) mode for each input signal of the UPFC, singular value decomposition (SVD) is used [35]. The minimum singular value $\sigma_{\min}$ is estimated over a wide range of operating conditions. For the SVD analysis, the total generated real power (which feeds the 2 existing loads and the transmission system losses in Figure 1) varies in the range of 0.1 to 5 pu, while the demand for a reactive load changes in 3 different states. At each operating point, the system model is linearized, the EM modes are identified, and the SVD-based controllability measurement is implemented. The capability of the UPFC inputs to control the EM modes over the specified range of operating conditions is shown in Figures 5–7. It is shown that the system loading increases the controllability of different inputs of the UPFC, and the EM mode controllability via δ_E is always higher than any other input.

9. Control system implementation

By using the linearized power system model and the PSO algorithm, interactions between the proposed controllers for the UPFC and MPSS controller are considered, and the controller's parameters are optimized simultaneously to achieve a global optimal damping behavior. The eigenvalue analysis and nonlinear time-domain simulations are used to validate the effectiveness of the proposed controller.

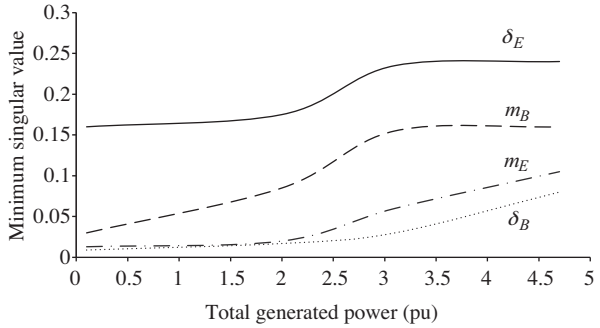

Figure 5. Minimum singular values with the UPFC inputs with respect to the load increase, at $Q_{L7} = 0.1$ (pu) and $Q_{L9} = 0.1$ (pu).

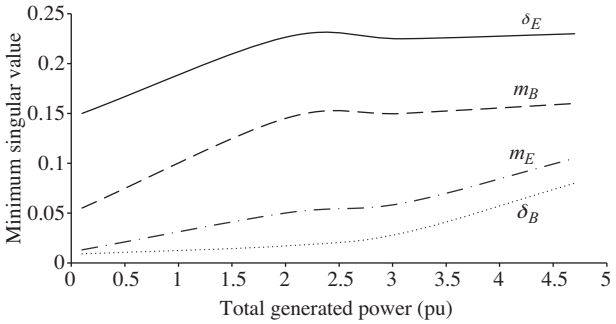

Figure 6. Minimum singular values with the UPFC inputs with respect to the load increase, at $Q_{L7} = 0.2$ (pu) and $Q_{L9} = 0.2$ (pu).

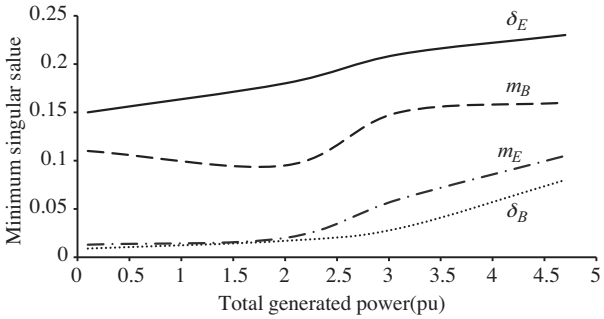

Figure 7. Minimum singular values with the UPFC inputs with respect to the load increase, at $Q_{L7} = 0.3$ (pu) and $Q_{L9} = 0.3$ (pu).

9.1. Concurrently attuned design using PSO

The proposed controller should be able to act well under all operating conditions, while an improvement for the damping of the critical modes is necessary. The selection of the controller's parameters is a complex optimization problem. Hence, to acquire an optimal combination, the PSO algorithm [36] is used to enhance the optimization problem. An optimization problem with respect to the eigenvalue-based objective function is used and the real part of the eigenvalue and damping ratio of the undamped electromechanical modes is constructed. The optimization problem is:

$$Minf(G_m, T_n) = af_1 + bf_2 \tag{28}$$

$$s.t \begin{array}{l} G_{m\min} \le G_m \le G_{m\max} \\ T_{n\min} \le T_n \le T_{n\max} \end{array},$$

where

$$f_1 = \sum_{j=1}^{N} \sum_{\xi_i \le \xi_0} (\xi_0 - \xi_{i,j})^2 \text{ and } f_2 = \sum_{j=1}^{N} \sum_{\sigma_i \ge \sigma_0} (\sigma_0 - \sigma_{i,j})^2. \tag{29}$$

Here, $\sigma_{i,j}$ and $\xi_{i,j}$ are the real part and damping ratio of the ith eigenvalue of the jth operating point, respectively. Parameters σ_0 and ξ_0 are the desired minimum real part and damping ratio that must be

achieved. Parameters G_m and T_n are the optimization parameters and $f(G_m,\ T_n)$ is the objective function, where m and n are the total number of gains and the time constants. The values of a and b are the weight factors for f_1 and f_2 with regard to the optimal point and are chosen to acquire better performance. In this paper, σ_0, ξ_0, a, and b are chosen as –2, 1, 5, and 10, respectively. Parameter N is the total number of operating points for which the optimization is performed. The PSO is employed to solve this optimization and search for an optimal set of power damping controller parameters. It is noted that this procedure leads to robust stabilization, while operating in a wide range of operating conditions. The optimization of the controller's parameters is performed by evaluating the objective function given in Eq. (28), which consists of multiple operating conditions. Table 4 gives the operating conditions and Table 5 presents the final values of the optimized parameters. The system eigenvalues with $\xi\langle 1$ and for 3 different cases, such as: a) base system, b) system with CUPFC (CUPFC with only P_{tie} as the controller input) and MPSS, and c) system with dual-layer UPFC and MPSS, are shown in Table 6. With these results, it is clear that the system damping is greatly improved with the dual-layer UPFC damping controller and MPSS.

Table 4. Three operating conditions (pu).

Operating condition	Case 1	Case 2	Case 3
P_1, Q_1	0.7778, 0.2056	0.5556, 0.2056	0.9911, 0.1722
P_2, Q_2	0.5556, 0.2611	0.5556, 0.2611	0.9444, 0.3944
P_3,Q_3	0.8020, 0.0697	1.3739, 0.1502	0.0095, 0.0712
P_4, Q_4	0.8889, 0.2244	0.5556, 0.2244	1.1111, 0.2222

Table 5. The optimal parameter tuning of the proposed controllers.

Controller parameters	Attuned design										
	CUPFC and MPSSs					Dual-layer UPFC & MPSSs					
	MPSS on generator 1		MPSS on generator 3		CUPFC	MPSS on generator 1		MPSS on generator 3		Dual-layer UPFC	
	ω input	p input	ω input	p input		ω input	p input	ω input	p input	First layer of the UPFC	Second layer of the UPFC
k	0.3164	0.4918	0.2083	0.5199	0.2429	5.0	0.4723	0.6213	0.1047	0.1646	0.5357
T_1	0.7093	0.7152	0.5539	0.9575	0.1742	0.6978	0.5322	0.7447	0.1465	0.8108	0.3489
T_2	0.4070	0.5836	0.5431	0.3039	0.5934	0.3123	0.0805	0.1318	0.3963	0.5185	0.5232
T_3	0.8589	0.6604	0.4522	0.6266	0.8263	0.6001	0.5142	0.0083	0.4223	0.4309	0.5045
T_4	0.3376	0.4465	0.5310	0.0478	0.5714	0.9292	0.5251	0.7392	0.7487	0.8843	0.1932

9.2. Nonlinear time-domain simulation

In order to show the performance of the proposed controller for the UPFC, simulation studies are performed using MATLAB/Simulink, as shown in Figure 8, and are verified by applying a 3-phase short-circuit fault with a 100-ms duration in the middle of one of the transmission lines, between buses 7 and 8, at $t = 1$ s. In this condition, the response with the attuned tuning of the dual-layer UPFC and MPSS damping controller is compared with the response of the attuned tuning of the CUPFC and MPSS damping controller. The interarea

and local mode of the swings with the attuned design of the CUPFC and MPSS damping controller and the dual-layer UPFC and MPSS damping controller are shown in Figures 9–11, where it is clearly seen that the simultaneous design of the dual-layer UPFC and MPSS damping controller significantly improves the stability performance of the test power system, and low-frequency swings are well damped out.

Table 6. Eigenvalues and damping ratios of the system before and after the attuned tuning with $\xi\langle 1$.

	Case 1		Case 2		Case 3	
	Eigenvalue	Damping ratio	Eigenvalue	Damping ratio	Eigenvalue	Damping ratio
Base system	−0.1744 ± i4.9583	−0.0352	−0.2364 ± i4.9271	−0.0479	0.0708 ± i4.8503	−0.0146
	−0.2682 ± i5.0935	0.0526	−0.2975 ± i5.1094	0.0581	−0.0974 ± i5.2225	0.0187
	−0.6350 ± i6.3493	0.0995	−0.7356 ± i6.4192	0.1139	−0.4646 ± i6.2046	0.0747
	−0.2333 ± i1.2513	0.1833	−0.2218 ± i1.2392	0.1761	−0.2440 ± i1.2732	0.1882
	−0.059 ± i0.0455	0.7914	−0.0489 ± i0.0514	0.6891	−0.0682 ± i0.0383	0.8721
	−1.3640 ± i0.2346	0.9855	−1.3012 ± i0.2718	0.9789	−1.6465 ± i0.2271	0.9906
CUPFC and MPSS	−3.618 ± i5.044	0.5829	−3.255 ±i6.060	0.4732	−3.432 ± i4.674	0.5918
	−3.684 ± i3.514	0.7236	−2.986 ±i4.042	0.5942	−3.508± i3.274	0.7340
	−0.3395 ± i0.2959	0.7539	−0.3331 ±i0.4487	0.5961	−0.3225 ± i0.2699	0.7668
	−0.11 ± i0.08	0.8195	−0.15 ±i0.1	0.8256	−0.1 ± i0.07	0.8180
	−0.0324 ± i0.0136	0.9216	−0.443 ± i0.193	0.9170	−0.299 ± i0.125	0.9234
	−0.24 ± i0.06	0.9738	−0.24 ± i0.05	0.9764	−0.24 ± i0.06	0.9728
Dual-layer UPFC and MPSS	−8.056 ± i6.367	0.7846	−7.207 ± i8.070	0.6661	−5.642 ± i5.986	0.6859
	−0.13 ± i0.09	0.8213	−7.117 ± i4.948	0.8210	−0.12 ± i0.09	0.8207
	−0.378 ± i0.163	0.9183	−0.17 ± i0.12	0.8235	−5.608 ± i3.588	0.8424
	−7.936 ± i2.216	0.9632	−0.6817 ± i0.3787	0.8742	−0.5348 ± i0.2543	0.9031
	−0.24 ± i0.05	0.9758	−0.479 ± i0.211	0.9153	−0.357 ± i0.152	0.9194
	−1.012 ± i0.0567	0.9984	−0.25 ± i0.05	0.9784	−0.24 ± i0.06	0.9750

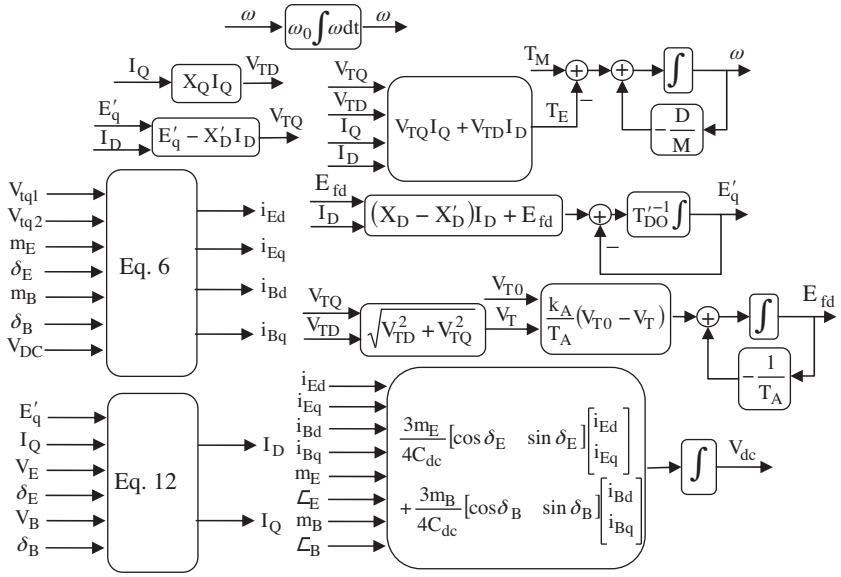

Figure 8. Nonlinear simulation of the test system.

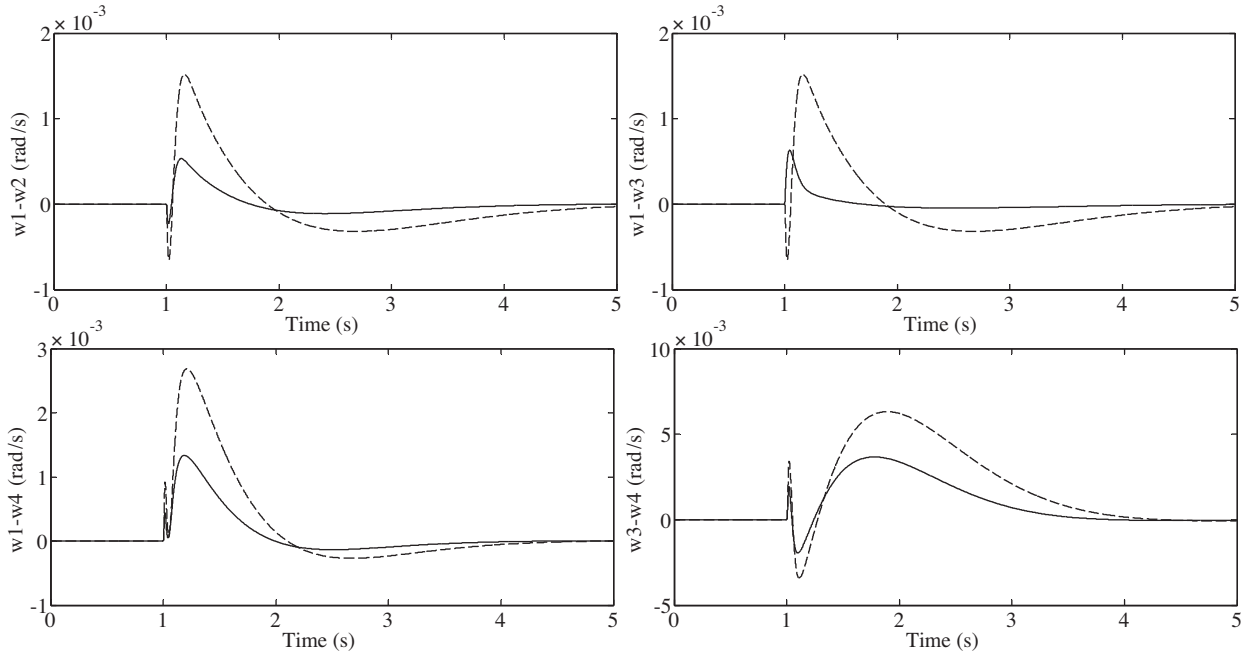

Figure 9. Local and interarea mode of the swings for case 1: solid (dual-layer UPFC and MPSS) and dashed (CUPFC and MPSS).

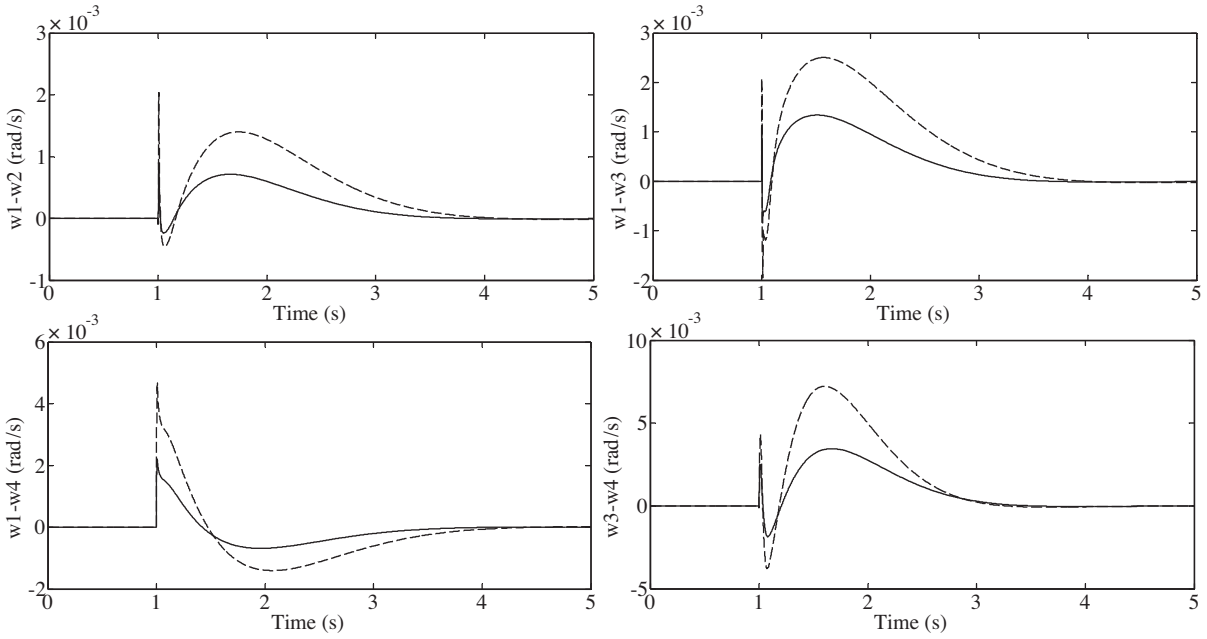

Figure 10. Local and interarea mode of the swings for case 2: solid (dual-layer UPFC and MPSS) and dashed (CUPFC and MPSS).

9.3. Delay-dependent stability

The power system model, excluding the WADC, is of the 38th order. By choosing ω_{13} as the output and u_g as the input (as shown in Figure 3), the Schur mode-reduction method [31] is utilized to achieve the reduced-order

system model. Figure 12 shows the frequency responses of the reduced-order and full-order systems. By the results, it is seen that with an order of more than 8, the frequency response of the reduced-order system is very close to that of the full-order system over the required frequency range (interarea mode with a frequency of 0.2–0.8 Hz and local mode with a frequency of 0.8–3 Hz). The parameters of the designed UPFC-WADC or the transfer function of H_{UPFC2} shown in Figure 3 are given as: $T_\omega = 5$, $T_1 = 0.3489$, $T_2 = 0.5232$, $T_3 = 0.5045$, and $T_4 = 0.1932$. Parameter K is a changing gain with the initial value $K = 0.5357$. To prevent the immoderate interface of the local mode, the output of the WADC is restricted by ± 0.08 pu. By electing sets of gain K and the rate of time-varying delay μ, the delay margin τ_d is computed based on the eighth-order reduced-order system model and WADC. The results are shown in Table 7. It can be seen that τ_d declines with the increase of K. Furthermore, for a fixed gain K, parameter τ_d declines with the increase in μ.

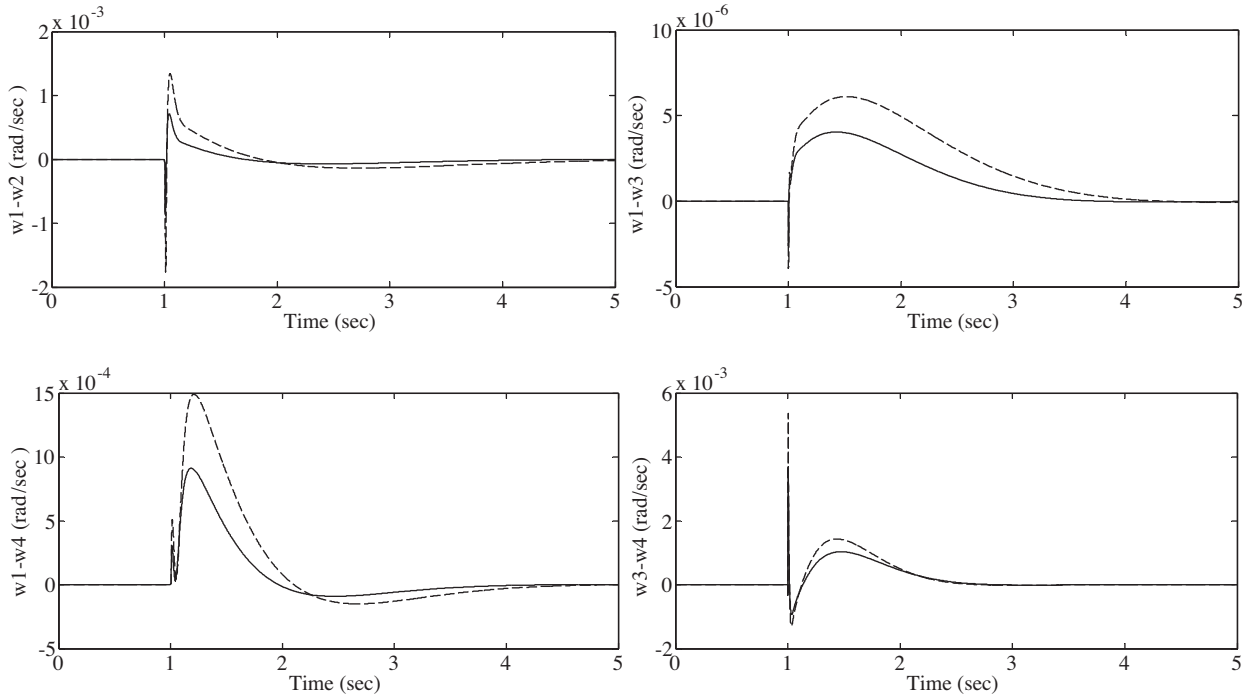

Figure 11. Local and interarea mode of the swings for case 3: solid (dual-layer UPFC and MPSS) and dashed (CUPFC and MPSS).

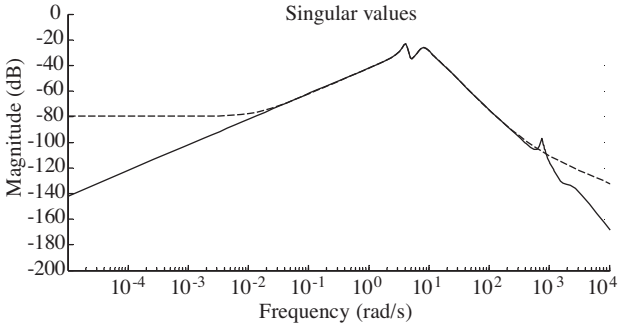

Figure 12. Frequency responses of the system: solid (full-order), dashed (reduced-order).

Table 7. Delay margin ($\mathcal{T}_d$/ms) influenced by the different gains of the UPFC-WADC.

k	$\mu = 0$	$\mu = 0.5$	$\mu = 0.9$
0.1	271.3	260.1	222.2
0.2	251.8	233.4	211.9
0.3	222.8	201.9	165.5
0.4	198.1	180.2	127.5
0.5357	169.4	158.2	108.9
0.5	155.2	128.6	95.5
0.6	113.5	91.3	81.1
0.7	102.1	83.4	75.9
0.8	89.7	75	62.2
0.9	55.9	49.3	45.3
1	47.4	42.3	33.2

10. Conclusion

The power system stability enhancement via coordination between MPSS and UPFC-based stabilizers has been discussed and investigated. In order to damp the power system interarea swings, a dual-layer control scheme for the UPFC has been proposed in multimachine systems. The first layer is achieved from the active power of the tie-line, as the local signal for the UPFC, and the second layer uses the wide-area or global signals, as additional measuring information from suitable remote network locations, where swings are well observable. By considering the minor information contained in the active power as the input of the conventional PSS, the damping of the low-frequency swing in the wide-area operation by the CPSS has little effectiveness. Hence, to solve this problem, a MPSS has been used to provide the control signals for the automatic voltage regulations to damp out swings through the machine's excitation systems that are placed at suitably selected generators. The coordination of MPSSs and the proposed UPFC controller over a wide range of loading conditions is presented as an optimization problem based on an objective function that is solved by the PSO algorithm. As the UPFC-WADC uses the communication links, a time-delay, dependent on these remote signals, has been considered for designing the UPFC-WADC, based on the Lyapunov theory and model reduction technique. The attuned design of the dual-layer UPFC and MPSS has been investigated and the results have been compared with the CUPFC and MPSS using a typical 2-area 4-machine benchmark power system. The simulation results show that under different operation conditions the coordination between the dual-layer UPFC and MPSS effectively damps system swings from the point of view of the settling time and overshoot.

Appendix A: description of the detailed model

The exciter, PSS, and UPFC parameters are:

Exciter: $\mathrm{k}_A = 20$; $\mathrm{T}_A = 0.05$;

MPSS: $\mathrm{T}_w = 10$; $\mathrm{T}_{i-\min} = 0.05$; $\mathrm{T}_{i-\max} = 1.5$; i = 1, 2, 3, 4; $\mathrm{G}_{\min} = 0$; $\mathrm{G}_{\max} = 100$; $\mathrm{T}_d = 0.01$;

UPFC: $\mathrm{x}_E = 0.1$; $\mathrm{x}_B = 0.1$; $\mathrm{K}_s = 1$; $\mathrm{T}_s = 0.05$; $\mathrm{C}_{DC} = 3$; $\mathrm{V}_{dc} = 2$; $\mathrm{m}_{E-\min} = 0$;

$\mathrm{m}_{E-\max} = 2$; $\mathrm{m}_{B-\min} = 0$; $\mathrm{m}_{B-\max} = 2$; $\mathrm{T}_w = 10$;

$\mathrm{T}_d = 0.01$; $\mathrm{T}_{i-\min} = 0.05$; $\mathrm{T}_{i-\max} = 1.5$; i = 1, 2, 3, 4; $\mathrm{G}_{\min} = 0$; $\mathrm{G}_{\max} = 100$;

References

[1] I. Kamwa, R. Grondin, G. Trudel, "IEEE PSS2B versus PSS4B: the limits of performance of modern power system stabilizers", IEEE Transactions on Power Systems, Vol. 20, pp. 903–915, 2005.

[2] K. Yoshimura, N. Uchida, "Multi input PSS optimization method for practical use by considering several operating conditions", IEEE Power Engineering Society Winter Meeting, Vol. 1, pp. 749–754, 1999.

[3] E. Rasooli Anarmarzi, M.R. Feyzi, M. Tarafdar Hagh, "Hierarchical fuzzy controller applied to multi-input power system stabilizer", Turkish Journal of Electrical Engineering & Computer Sciences, Vol. 18, pp. 541–551, 2010.

[4] X.P. Zhang, C. Rehtanz, B. Pal, Flexible AC Transmission Systems: Modelling and Control, Berlin Heidelberg, Springer Verlag, 2006.

[5] Y.H. Song, A.T. Johns, Flexible AC Transmission Systems (FACTS), London, The Institution of Electrical Engineers, 1999.

[6] S. Jiang, A.M. Gole, U.D. Annakkage, D. Jacobson, "Damping performance analysis of IPFC and UPFC controllers using validated small-signal models", IEEE Transactions on Power Delivery , Vol. 26, pp. 446–454, 2011.

[7] A. Phadke, M. Fozdar, K. Niazi, "Robust tuning of fixed-parameter static VAR compensator controller for damping inter-area oscillations in power system", Electric Power Components and Systems, Vol. 38, pp. 974–995, 2010.

[8] S. Morsli, A. Tayeb, D. Mouloud, C. Abdelkader, "A robust adaptive fuzzy control of a uni?ed power ?ow controller", Turkish Journal of Electrical Engineering & Computer Sciences, Vol. 20, pp. 87–98, 2012.

[9] L.J. Cai, I. Erlich, "Simultaneous coordinated tuning of PSS and FACTS damping controllers in large power systems", IEEE Transactions on Power Systems, Vol. 20, pp. 294–300, 2005.

[10] T. Nguyen, R. Gianto, "Neural networks for adaptive control coordination of PSSs and FACTS devices in multi-machine power system", IET Generation, Transmission & Distribution, Vol. 2, pp. 355–372, 2008.

[11] T. Nguyen, R. Gianto, "Optimisation-based control coordination of PSSs and FACTS devices for optimal oscillations damping in multi-machine power system", IET Generation, Transmission & Distribution, Vol. 1, pp. 564–573, 2007.

[12] J.M. Ramirez, R.J. Davalos, V. Valenzuela, "Coordination of FACTS-based stabilizers for damping oscillations", IEEE Power Engineering Review, Vol. 20, pp. 46–49, 2000.

[13] X. Lei, E.N. Lerch, D. Povh, "Optimization and coordination of damping controls for improving system dynamic performance", IEEE Transactions on Power Systems, Vol. 16, pp. 473-480, 2001.

[14] M.E. Aboul-Ela, A.A. Sallam, J.D. McCalley, A.A. Fouad, "Damping controller design for power system oscillations using global signals", IEEE Transactions on Power Systems, Vol. 11, pp. 767–773, 1996.

[15] I. Kamwa, J. Beland, G. Trudel, R. Grondin, C. Lafond, D. McNabb, "Wide-area monitoring and control at Hydro-Québec: past, present and future", IEEE Power Engineering Society General Meeting, Vol.1, pp 1–12, 2006.

[16] J.H. Chow, J.J. Sanchez-Gasca, H. Ren, S. Wang, "Power system damping controller design-using multiple input signals", IEEE Control Systems Magazine, Vol. 20, pp. 82–90, 2000.

[17] I. Kamwa, A. Heniche, G. Trudel, M. Dobrescu, R. Grondin, D. Lefebvre, "Assessing the technical value of FACTS-based wide-area damping control loops", IEEE Power Engineering Society General Meeting, Vol. 2, pp. 1734–1743, 2005.

[18] N.R. Chaudhuri, A. Domahidi, R. Majumder, B. Chaudhuri, P. Korba, S. Ray, K. Uhlen, "Wide-area power oscillation damping control in Nordic equivalent system", IET Generation, Transmission & Distribution, Vol. 4, pp. 1139–1150, 2010.

[19] J. De La Ree, V. Centeno, J.S. Thorp, A.G. Phadke, "Synchronized phasor measurement applications in power systems", IEEE Transactions on Smart Grid, Vol. 1, pp. 20–27, 2010.

[20] I. Kamwa, R. Grondin, Y. Hebert, "Wide-area measurement based stabilizing control of large power systems-a decentralized/hierarchical approach", IEEE Transactions on Power Systems, Vol. 16, pp. 136–153, 2001.

[21] H. Ni, G.T. Heydt, L. Mili, "Power system stability agents using robust wide area control", IEEE Transactions on Power Systems, Vol. 17, pp. 1123–1131, 2002.

[22] B. Naduvathuparambil, M.C. Valenti, A. Feliachi, "Communication delays in wide area measurement systems", Proceedings of the 34th Southeastern Symposium on System Theory, Vol. 2, pp. 118–122, 2002.

[23] P. Kundur, Power System Stability and Control, New York, McGranw-Hill, 1994.

[24] H. Wang, "Applications of modelling UPFC into multi-machine power systems", IEE Proceedings - Generation, Transmission and Distribution, Vol. 146, pp. 306–312, 1999.

[25] Y. Hashemi, R. Kazemzadeh, M.R. Azizian, A. Sadeghi, "Simultaneous coordinated design of two-level UPFC damping controller and PSS to damp oscillation in multi-machine power system", 26th International Power System Conference, pp 1–13, 2011.

[26] X. Yang, A. Feliachi, "Stabilization of inter-area oscillation modes through excitation systems", IEEE Transactions on Power Systems, Vol. 9, pp. 494–502, 1994.

[27] X. Yang, A. Feliachi, R. Adapa, "Damping enhancement in the Western US power system: a case study", IEEE Transactions on Power Systems, Vol. 10, pp. 1271–1278, 1995.

[28] A.F. Snyder, D. Ivanescu, N. HadjSaid, D. Georges, T. Margotin, "Delayed-input wide-area stability control with synchronized phasor measurements and linear matrix inequalities", IEEE Power Engineering Society Summer Meeting, Vol. 2, pp. 1009–1014, 2000.

[29] H. Wu, K.S. Tsakalis, G.T. Heydt, "Evaluation of time delay effects to wide-area power system stabilizer design", IEEE Transactions on Power Systems, Vol. 19, pp. 1935–1941, 2004.

[30] W. Yao, L. Jiang, Q. Wu, J. Wen, S. Cheng, "Delay-dependent stability analysis of the power system with a wide-area damping controller embedded", IEEE Transactions on Power Systems, Vol. 26, pp. 233–240, 2011.

[31] M. Safonov, R. Chiang, "A Schur method for balanced-truncation model reduction", IEEE Transactions on Automatic Control, Vol. 34, pp. 729–733, 1989.

[32] A. Sedaghati, "A PI controller based on gain-scheduling for synchronous generator", Turkish Journal of Electrical Engineering & Computer Sciences, Vol. 14, pp. 241–251, 2006.

[33] S. Liu, A. Messina, V. Vittal, "A normal form analysis approach to siting power system stabilizers (PSSs) and assessing power system nonlinear behavior", IEEE Transactions on Power Systems, Vol. 21, pp. 1755–1762, 2006.

[34] K. Sebaa, H. Gueğguen, M. Boudour, "Mixed integer non-linear programming via the cross-entropy approach for power system stabilisers location and tuning", IET Generation, Transmission & Distribution, Vol. 4, pp. 928–939, 2010.

[35] D. Yang, C. Rehtanz, Y. Li, D. Cai, "Identification of dominant oscillation mode using complex singular value decomposition method", Electric Power Systems Research, Vol. 83, pp. 227–236, 2011.

[36] Y. Abdel-Magid, M. Abido, "Optimal multiobjective design of robust power system stabilizers using genetic algorithms", IEEE Transactions on Power Systems, Vol. 18, pp. 1125–1132, 2003.